

A cryptic record of magma mixing in diorites revealed by high-precision SIMS oxygen isotope analysis of zircons

S.K. Appleby ^{a,*}, C.M. Graham ^a, M.R. Gillespie ^b, R.W. Hinton ^a, G.J.H. Oliver ^c, EIMF ^d

^a *Grant Institute of Earth Science, University of Edinburgh, West Mains Road, Edinburgh, EH9 3JW, UK*

^b *British Geological Survey, Murchison House, West Mains Road, Edinburgh, EH9 3LA, UK*

^c *School of Geography & Geosciences, Crustal Geodynamics Group, University of St. Andrews, St. Andrews, KY16 9AL, UK*

^d *Edinburgh Ion Microprobe Facility, University of Edinburgh, West Mains Road, Edinburgh, EH9 3JW, UK*

Abstract

High-precision in-situ ion microprobe (SIMS) oxygen isotope analysis of zircons from two diorite intrusions associated with the late Caledonian Lochnagar pluton in Scotland has revealed large differences in the degree of heterogeneity in zircon $\delta^{18}\text{O}$ between the diorites. Zircon crystals from the Cul nan Gad diorite (CnG) show a unimodal distribution of oxygen isotope values ($\delta^{18}\text{O} = 6.0 \pm 0.6 \text{‰}$ (2σ)) and no or only minor grain-scale variation. Those from the Allt Darrarie diorite (AD1) show a large range in $\delta^{18}\text{O}$ and an apparent bimodal distribution with modes of $6.6 \pm 0.4 \text{‰}$ and $7.3 \pm 0.4 \text{‰}$. Variations of up to 1.2 ‰ occur between and within grains; both an increase and decrease in $\delta^{18}\text{O}$ with zircon growth has been observed. The $\delta^{18}\text{O}$ composition of growing zircon can only change, if open-system processes affect the magma composition, i.e. if material of contrasting $\delta^{18}\text{O}$ composition is added to the magma. The variability in AD1 is interpreted to represent a cryptic record of magma mixing. A 'deep crustal hot zone' is a likely site for generation of the dioritic magmas which developed by mixing of residual melts and crustal partial melts or by melting of mafic lower crustal rocks. The overall small number of zircons with mantle-like $\delta^{18}\text{O}$ values ($5.3 \pm 0.6 \text{‰}$ (2σ)) in the Lochnagar diorites are largely the products of crustal differentiation rather than crustal growth.

The $\delta^{18}\text{O}$ of quartz from the CnG and AD1 diorites shows only minor variation (CnG: $10.9 \pm 0.5 \text{‰}$ (2σ), AD1: $11.7 \pm 0.6 \text{‰}$ (2σ)) within single populations, with no evidence of mixing. Quartz-zircon isotopic disequilibrium is consistent with later crystallisation of quartz from late magmatic fluids, and in case of the AD1 diorite after the inferred magma mixing from a homogenised, higher $\delta^{18}\text{O}$ melt.

36 High-precision SIMS oxygen isotope analysis of zircon provides a new approach to
37 identifying and resolving previously undetected early-stage magma mixing and constraining
38 the compositions and origins of the component magmas. A combination of zircon, quartz and
39 whole-rock data has proven to be a powerful tool in reconstructing the petrogenetic evolution
40 of diorite from early crystallisation to late alteration.

41

42

43 *Keywords:* oxygen isotopes; zircon; diorite; magma mixing; SIMS

44

45 * Corresponding author. Tel.: +44 131 6504849; fax: +44 131 6683184.

46 *Email addresses:* sarah.k.appleby@gmail.com (S.K. Appleby), Colin.Graham@ed.ac.uk

47 (C.M. Graham), mrg@bgs.ac.uk (M.R. Gillespie), Richard.Hinton@ed.ac.uk (R.W. Hinton),

48 gjho@st-andrews.ac.uk (G.J.H. Oliver)

49

50

51 **1. Introduction**

52

53 Oxygen isotopes have been widely used in petrogenetic evolution studies of granitic rocks
54 to constrain the relative contributions of mantle and crust and the roles of fractional
55 crystallisation, assimilation and magma mixing. The oxygen isotope compositions of granites
56 and their constituent minerals are sensitive to modification by assimilation of ^{18}O -enriched
57 crustal rocks, magma mixing and/or hydrothermal alteration by ^{18}O -depleted fluids (e.g. King
58 et al., 1997, 2000; Monani and Valley, 2001; Valley and Graham, 1996).

59 Zircon is a common accessory mineral in intermediate and silicic plutonic rocks. Due to
60 extremely slow rates of oxygen diffusion and high closure temperatures (Dodson, 1973; Peck
61 et al., 2003; Valley, 2003; Watson and Cherniak, 1997) it is insensitive to hydrothermal
62 alteration and fractional crystallisation during cooling, and therefore retains its oxygen isotope
63 composition from the time of crystallisation (e.g. Kemp et al., 2005a, 2005b, 2006, 2007;
64 King et al., 1998, 2002, 2004; King and Valley, 2001; Lackey et al., 2005, 2006). New
65 developments in micro-analytical techniques now permit the rapid in-situ analysis of oxygen
66 isotopes in zircon at high precision (here 0.4-0.6 ‰ (2σ)) by ion microprobe. With a beam
67 diameter of only c. 20 μm , multiple analyses may be made in a single zircon crystal, which
68 enables detection of differences in $\delta^{18}\text{O}$ between growth zones and between cores and rims in
69 individual crystals, and allows detailed comparison between crystals. The high analytical
70 precision and high spatial resolution of modern ion microprobes offers the potential to
71 identify previously undetectable variations in oxygen isotope composition, providing more
72 detailed insights into granite magma genesis and evolution.

73 Quartz, which commonly crystallises in the later stages of magmatic evolution, is also
74 more resistant to isotopic modification than its host rock, and hence may also preserve
75 isotopic signatures derived directly from the melt (e.g. Bindeman and Valley, 2001; Criss and
76 Taylor, 1986; Monani and Valley, 2001; Valley et al., 1994). Conventional laser fluorination
77 oxygen isotope data have commonly been used to assess the state of equilibrium between
78 zircon, quartz and whole-rock samples in silicic magmatic rocks as a useful guide to the
79 petrological and geochemical evolution of magmas and rocks (King et al., 1997, 1998, 2001,
80 2004; Lackey et al., 2005, 2006; Monani and Valley, 2001).

81 This paper presents high-precision in-situ ion microprobe oxygen isotope data for zircon
82 and quartz, supported by whole-rock $\delta^{18}\text{O}$ analyses, from two diorite intrusions forming part
83 of the late Caledonian (424-413 Ma) (Appleby et al. 2007, unpublished data) Lochnagar
84 pluton in Scotland. It introduces a new approach to deciphering the detailed grain-scale

85 petrogenetic information stored in zircon and quartz, and tests the results against recent
86 models for the generation and evolution of intermediate and silicic calc-alkaline igneous rocks
87 (e.g. Annen et al., 2006).

88

89

90 **2. Geological background and sample details**

91

92 The Lochnagar pluton, which crops out over an area of c. 150 km², is located in the
93 Grampian Highlands of Scotland and belongs to the classic suite of late Caledonian ‘I-type’
94 intrusions that were emplaced at 430-400 Ma, after the c. 470 Ma Grampian Event and
95 broadly contemporaneously with the oblique collision of Baltica and Laurentia (the Scandian
96 Event) (Coward, 1990; Dallmeyer et al., 2001; Dewey and Mange, 1999; Kinny et al., 2003).
97 However, the connection between this collision and the voluminous I-type magmatism is
98 unclear. Based on field relationships and whole-rock geochemical and isotopic data, the
99 Lochnagar pluton has been described as composite, comprising three main granite facies (L1,
100 L2, L3) distinguished by textural and modal variations, a late intrusion of microgranite, and
101 several marginal intrusions of diorite (Fig. 1) (Halliday, 1984; Halliday et al., 1979;
102 Oldershaw, 1974; Smith et al., 2001). Two small diorite intrusions, Cul nan Gad (CnG) and
103 Allt Darrarie (AD1) (with areal dimensions of 4-5 x 1.8 km (CnG) and 0.6 x 0.4 km (AD1);
104 Smith et al. 2001), are the subject of this study. Based on field relationships these were
105 interpreted to be consanguineous with, but cut by, the granite (Smith et al. 2001).

106 The diorites are dark grey, fine- to medium-grained (< 1-3 mm), and have a calc-alkaline
107 metaluminous composition. They comprise plagioclase (45-50 %), biotite (c. 40 %),
108 hornblende (< 5-10 %) and interstitial quartz (c. 5 %), with accessory ilmenite and magnetite,
109 titanite (absent in CnG), zircon and apatite. All minerals are distributed evenly, which
110 suggests that they do not contain cumulate or restite material and that the diorites represent
111 melt compositions. Plagioclase crystals are sometimes zoned, commonly twinned and weakly
112 altered to sericite in the centre. Biotites are often partially or entirely altered to chlorite, which
113 is particularly prominent in the CnG diorite.

114

115

116 **3. Methodology**

117

118 *3.1. Zircon sample preparation*

119

120 Zircon separation was carried out at the University of St. Andrews Mineral Separation
121 Facility. Rock samples of approximately 5 kg were crushed and sieved to obtain the < 500 µm
122 fraction from which zircon crystals were separated using a Wilfley Table, heavy liquids and a
123 Frantz magnetic separator. Approximately 100 zircon crystals were hand-picked from the
124 remaining heavy, non-magnetic fraction, providing a range of grain size, morphology,
125 transparency, alteration and occurrence of inclusions or cracks. The crystals were mounted
126 into epoxy (Araldite) and the zircon mounts polished to about half thickness to expose the
127 crystal interiors. The polished surfaces were imaged in back-scattered electron (BSE) and
128 cathodoluminescence (CL) mode using a Philips XL30CP Scanning Electron Microscope
129 (SEM) at the University of Edinburgh to identify internal zoning features, inherited material,
130 inclusions and cracks. Suitable crystals for in-situ oxygen isotope analysis were selected using
131 this information.

132

133 *3.2. Zircon SIMS oxygen isotope analysis*

134

135 Zircon oxygen isotope data were obtained using a Cameca ims-1270 ion microprobe at the
136 University of Edinburgh following the methods of Cavosie et al. (2005) and Kemp et al.
137 (2006). A 6nA primary $^{133}\text{Cs}^+$ ion beam with a diameter of c. 20 µm was used, charge was
138 neutralised using a normal-incidence electron gun, secondary ions were extracted at 10 kV
139 Köhler illumination, and $^{18}\text{O}^-$ and $^{16}\text{O}^-$ ions were monitored simultaneously on dual Faraday
140 cups. Pre-sputtering for 45 seconds and subsequent data collection over ten cycles resulted in
141 a total acquisition time of c. 210 seconds. The secondary yield of ^{18}O under these conditions
142 was typically between 4.5×10^6 and 5.5×10^6 counts per second. To correct for instrumental
143 mass fractionation (IMF) and instrumental drift, all data were normalised to zircon standard
144 91500 ($\delta^{18}\text{O} = 9.86 \text{ ‰}$) (Wiedenbeck et al., 2004), which was analysed in blocks of 5 to 10
145 after every 10 to 15 unknown zircon analyses. During stable instrument conditions the
146 unknown zircon analyses were normalised to the daily average $^{18}\text{O}/^{16}\text{O}$ value obtained for
147 91500. In cases where significant instrumental drift was recognised, the analytical conditions
148 changed or sample exchange was carried out, the data were divided into sessions in which
149 unknowns were normalised to the linearly interpolated $^{18}\text{O}/^{16}\text{O}$ value derived from analyses of
150 the bracketing 91500 standard.

151 Prior to oxygen isotope analysis, HfO_2 concentrations in the zircons were measured by
152 electron microprobe as variations in HfO_2 have been shown to cause variations in IMF (Peck

153 et al., 2001). This has been shown to be particularly important when conducting analysis
154 using e.g. a Cameca ims-4f at high-energy offset. However, in this study oxygen isotope
155 analysis were carried out using a Cameca ims-1270 ion microprobe, and in both diorite
156 samples HfO₂ variations in zircons were ≤ 0.5 wt %; therefore corrections for IMF were
157 unnecessary. The internal precision of individual point analyses based on counting statistics
158 varied between 0.1-0.2 ‰. External precision based on the reproducibility of standard 91500
159 ranged from 0.4 ‰ (n=57) to 0.6 ‰ (n=38) (2SD) and 0.040 to 0.087 (1 s.e.m.).

160 Analyses were conducted in clear, crack- and inclusion-free areas of representative zircon
161 crystals. Where possible, multiple analyses (core to rim) were carried out on single zircon
162 crystals to document zircon growth histories, and occasionally also in adjacent spots within
163 crystals to assess reproducibility. The ion probe pits were subsequently imaged in BSE and
164 Secondary Electron mode using an SEM to determine the exact position of the analyses and to
165 ensure that no cracks in the bottom of the pit might have influenced the results. Data obtained
166 from suspect locations were rejected. In addition, data were excluded when the correction on
167 the position of the secondary ion beam was anomalously large.

168

169 3.3. Quartz SIMS oxygen isotope analysis

170

171 Oxygen isotope analysis of quartz was also carried out on polished thin sections using the
172 Cameca ims-1270 ion microprobe, employing the same instrument set-up as for zircon
173 oxygen isotope analysis. Quartz data were normalised to quartz standard NBS28 ($\delta^{18}\text{O} = 9.58$
174 ‰) (National Institute of Standards & Technology), which was analysed after every 15-20
175 unknowns. Internal precision calculated from NBS28 varied between 0.1 ‰ and 0.2 ‰. The
176 external precision was 1.1 ‰ (2SD, n=59) and 0.072 (1 s.e.m.). In comparison, uncertainties
177 on the unknowns were considerably lower (0.5 ‰ (n=22) and 0.6 ‰ (n=27) (2SD), 0.057 (1
178 s.e.m.) for CnG and AD1 respectively). Thus, the uncertainties on the unknown quartz
179 crystals most closely reflect the analytical precision.

180 Where possible, multiple ion microprobe analyses were obtained between the centre and
181 edge of each crystal in order to identify potential oxygen isotope zoning arising either from
182 changes in the magma chemistry or from oxygen volume diffusion.

183

184 3.4. Whole-rock analyses

185

186 Oxygen isotope analyses of whole-rock samples were carried out at the Scottish
187 Universities Environmental Research Centre (SUERC) at East Kilbride following the
188 Macaulay et al. (2000) modification of the laser fluorination methodology of Sharp (1990).
189 Approximately 1 mg of powdered sample was reacted with ClF_3 whilst being heated with a
190 CO_2 laser. The resultant oxygen was purified, converted to CO_2 on platinised graphite, and the
191 yield measured with a capacitance manometer. The oxygen isotope composition of the CO_2
192 was measured by a Micromass PRISM 3 dual inlet, triple collector mass spectrometer with a
193 working standard gas calibrated against international reference materials. The accuracy and
194 precision are $\pm 0.4 \text{ ‰}$ (2σ), and NBS28 gives a value of 9.56 ‰ .

195 Major element concentrations were determined at the University of Edinburgh using a
196 PANalytical PW2404 wavelength-dispersive sequential X-ray spectrometer.

197

198

199 **4. Results**

200

201 *4.1. Zircon description*

202

203 Zircon crystals show a similar range of sizes, morphologies and internal zoning textures in
204 both diorites. This is a common phenomenon and is generally interpreted to be the result of
205 varying local kinetic factors such as diffusion rates and adsorption (Dowty, 1980; Vavra,
206 1990, 1993). The only obvious difference between CnG and AD1 zircons lies in their CL
207 character. AD1 zircons are overall more strongly luminescent and usually show only smaller
208 luminescence contrast between growth zones.

209 In both diorite samples zircons vary in size between c. $200 \mu\text{m}$ and $\geq 700 \mu\text{m}$ along the c-
210 axis, and have equant, stubby and elongated morphologies (aspect ratios AD1: $1:1.1$ to $1:\geq 5.6$,
211 CnG: $1:1.2$ to $1:1:\geq 7.3$) with stubby and elongated crystals being dominant. With respect to
212 internal zoning, all zircons consist of a core, which usually comprises most of the crystal, and
213 up to three mantles and a rim varying in width from c. $5 \mu\text{m}$ to $100 \mu\text{m}$. Cores, mantles and
214 rims, are separated by resorption surfaces, which are generally interpreted to reflect periods of
215 Zr undersaturation in the magma for which the dominant controls are either large-scale
216 mixing events or local kinetic phenomena (Corfu et al., 2003). U-Pb dating by ion microprobe
217 has shown that none of these cores contains inherited (significantly older) components.
218 Hence, they represent magmatic cores that precipitated from the diorite magma, but reflect a
219 different (early) evolution stage than the surrounding rims. Magmatic cores are either

220 completely unzoned (c1) (Fig. 2a), comprise a relatively large inner unzoned domain (c1) and
221 a surrounding outer oscillatory zoned domain (c2) (Fig. 2b-d) or appear to be entirely zoned
222 (c2) (Fig. 2e). In the latter case a c1 domain is usually either difficult or impossible to
223 identify. In terms of CL intensity, c1 domains are always moderately to weakly luminescent,
224 whereas zones within the c2 domain vary between strongly and weakly luminescent. Mantles
225 and rims consist of either a single or multiple zones.

226 Based on these characteristics it is likely that both diorites contain only a single zircon
227 population in which c1, c2 and the surrounding mantles and rims vary in size due to local
228 differences in growth rate or Zr saturation level in the magma.

229

230 *4.2. Zircon oxygen isotope data*

231

232 All oxygen isotope values reported here are in per mil (‰) and relative to VSMOW
233 (Vienna Standard Mean Ocean Water). Oxygen isotope data are presented in Figures 3a and
234 4a as histograms with overlaid cumulative probability curves, which were calculated by
235 summing the probability distributions of a suite of data with normally distributed errors
236 (Isoplot ver.3.00, Ludwig, 2003). The bin widths of the histograms were chosen according to
237 the precision (1σ) obtained from analyses of standard 91500 in the same analytical session, as
238 this best represents the instrument performance during each session. Heterogeneities larger
239 than those detected in 91500, which is assumed to be homogeneous in $\delta^{18}\text{O}$, are considered to
240 reflect real variations in oxygen isotope composition. The data are also shown in grain-scale
241 variation plots (Fig. 3c & 4c) to establish whether heterogeneities mainly occur between or
242 within grains; these diagrams also illustrate whether the data lie within the error of the mean.

243 The $\delta^{18}\text{O}$ values of zircons from CnG lie between 5.5 ‰ and 6.4 ‰, with a mean value of
244 6.0 ‰ (n=36) and a standard deviation of 0.6 ‰ (2SD) (Table 1, Appendix 1). Zircon
245 standard 91500 analysed in the same analytical session displays the same standard deviation
246 (n=38) and degree of heterogeneity (2SD = 0.6 ‰). From this we interpret that the analytical
247 precision of this session approximates 0.6 ‰ (2σ). The cumulative probability-histogram for
248 CnG (Fig. 3a) shows a unimodal distribution with a mode of 5.9 ‰; a similar distribution is
249 observed for 91500. Neither intra-grain and inter-grain variations in $\delta^{18}\text{O}$ nor systematic
250 differences between cores, mantles and rims were detected (Fig. 3b). The grain-scale variation
251 plot (Fig. 3c) reveals that all analyses lie within 2σ error of the mean and that only minor
252 variation exists between and within crystals. However, these variations are not resolvable
253 within the limits of analytical uncertainty.

254 Zircons from AD1 are relatively enriched in ^{18}O and display a much larger range in $\delta^{18}\text{O}$
255 than those from CnG, ranging from 6.1 ‰ to 8.1 ‰ with a mean of 7.1 ‰ (n=41). A standard
256 deviation of 0.9 ‰ (2SD) is more than twice as large as for the 91500 standard analysed in
257 the same analytical session (0.4 ‰, 2SD, n=57) and must therefore be considered to represent
258 real isotopic heterogeneity. The cumulative probability-histogram (Fig. 4a) shows an apparent
259 bimodal distribution with partly overlapping modes of 6.6 ‰ and 7.3 ‰. Based on this
260 observation the data were separated into two apparent oxygen isotope populations with mean
261 $\delta^{18}\text{O}$ values of 6.6 ± 0.4 ‰ (population 1, 2σ) and 7.4 ± 0.4 ‰ (population 2, 2σ). Plotting the
262 probability-histogram of the same data separated into c1, c2 core domains, and mantles and
263 rims (Fig. 4b) shows that each textural component (cores, rims etc.) also displays a bimodal
264 distribution. Thus, bimodality in AD1 cannot be attributed to systematic intra-grain
265 differences or zonations in $\delta^{18}\text{O}$. The grain-scale variation plot reveals that, as indicated by
266 the cumulative probability-histogram, several values lie above and below the field defining
267 the 2σ error of the mean for the whole AD1 data set (Fig. 4c). It also demonstrates that the
268 large range in values results from variations both between grains (e.g. grain 16: 6.1-6.5 ‰,
269 grain 11: 7.2-8.1 ‰) and within grains (core-mantle/rim, c1-c2 core domains and even within
270 core domains). The largest *intra-grain* variation of 1.2 ‰ in grain 10 occurs between c1 (7.8
271 ‰) and c2 (6.6 ‰) core domains, and represents only about half of the full range of variation
272 of $\delta^{18}\text{O}$ in AD1 zircons. The largest variation *between a magmatic core and rim* can be
273 observed in grain 11 (0.9 ‰) (core: 7.2 ‰, rim: 8.1 ‰) (Fig. 2a) and the largest range *within*
274 *a single domain* in grain 9 (c2a: 6.5‰, c2b: 7.3‰) (Fig. 2b). This demonstrates that changes
275 in $\delta^{18}\text{O}$ do not always conform to occurrence of resorption surfaces, but also exist within a
276 single zone. Evidence was also found of cores and rims in some zircon crystals showing no -
277 only minor - intra-grain variations, such as grain 5 (core: 7.4 ‰, rim: 7.5‰), despite being
278 separated by resorption surfaces (Fig. 2c). Commonly AD1 zircon crystals show an increase
279 in $\delta^{18}\text{O}$ with zircon growth in grains where multiple analyses (core to rim) were carried out,
280 but grain 10 very clearly displays the opposite trend (Fig. 2d).

281

282 4.3. Quartz oxygen isotope data

283

284 In both intrusions, quartz crystals from tens of microns to approximately 1 mm are weakly
285 to moderately luminescent. Almost all crystals have annealed and open cracks, with typically
286 more weakly luminescent areas along them (Fig. 5); these are a common feature in quartz

287 crystals (e.g. Valley and Graham, 1996). CL evidence of growth zoning was not generally
288 observed, but numerous crystals have weakly luminescent rims.

289 CnG quartz oxygen isotope data range from 10.4 ‰ to 11.4 ‰ with a mean of 10.9 ± 0.5
290 ‰ (2σ , $n=22$) (Table 1, Appendix 2). One analysis in a weakly luminescent (possibly
291 hydrothermally altered) area yields a value of 12.0 ‰. AD1 quartz oxygen isotope values
292 range from 11.3 ‰ to 12.3 ‰ with a mean of 11.7 ± 0.6 ‰ (2σ , $n=27$). The values from both
293 samples display unimodal distributions (Fig. 7), and all data other than the possibly altered
294 sample lie within error of the mean. A systematic change in composition between grain
295 centres and rims or between grain sizes was not observed.

296

297

298 **5. Discussion**

299

300 The results of this study show that zircon crystals from the Lochnagar diorites display
301 significant differences in their degree of isotopic heterogeneity. All zircons from the CnG
302 diorite sample are homogeneous (within 2σ error of the mean) in their oxygen isotope
303 composition, with a population mean of 6.0 ± 0.6 ‰ (2σ). Those from the AD1 diorite are
304 heterogeneous and yield two apparent populations of 6.6 ± 0.4 ‰ and 7.4 ± 0.4 ‰.

305 Comparison of the $\delta^{18}\text{O}$ of zircons with those of co-existing quartz and their host whole-
306 rocks may be used to assess whether any of the oxygen isotope populations revealed in zircon
307 are in isotopic equilibrium with either quartz or host rocks. In addition, it enables us to resolve
308 the contrasting magmatic evolution and processes of the two diorites in more detail.

309

310 *5.1. Whole-rock – zircon equilibrium fractionation*

311

312 Equilibrium oxygen isotope fractionation factors between whole-rock and zircon $\Delta(\text{WR-Zrc})$
313 vary systematically with temperature and SiO_2 concentration (Valley et al., 1994, 2005).

314 Higher silica concentrations in more evolved rocks reflect higher abundances of quartz and
315 feldspar, which are enriched in ^{18}O relative to zircon and responsible for higher whole-rock
316 $\delta^{18}\text{O}$ values. Hence, $\Delta(\text{WR-Zrc})$ at any temperature increases with increasing whole-rock
317 SiO_2 content. Differentiation in magmas therefore has no measurable effect on $\delta^{18}\text{O}$ values in
318 zircon (Valley et al., 1994). At magmatic temperatures, equilibrium values for $\Delta(\text{Zrc-WR})$
319 range from ~ -0.5 ‰ for mafic rocks to ~ -2.0 ‰ for granites according to the relationship
320 (Lackey, 2005; Valley et al., 1994, 2005):

321

$$\Delta^{18}\text{O}(\text{Zrc-WR}) = \delta^{18}\text{O}(\text{Zrc}) - \delta^{18}\text{O}(\text{WR}) \sim -0.0612(\text{wt}\% \text{SiO}_2) + 2.5 \quad (1)$$

323

324 For the CnG diorite ($\delta^{18}\text{O}(\text{WR}) = 7.2 \pm 0.4 \text{‰}$ (n=2); $\text{SiO}_2(\text{WR}) = 54.6 \text{ wt}\%$; $\delta^{18}\text{O}(\text{Zrc})$
325 $= 6.0 \pm 0.6 \text{‰}$) $\Delta(\text{Zrc-WR})$ values lie between -1.8‰ and -0.6‰ (taking the error on the
326 analyses into account), which is in agreement with a calculated equilibrium $\Delta(\text{Zrc-WR})$ of -
327 0.8. Thus, CnG zircons appear to be in isotopic equilibrium with their host rock (Fig. 6).

328 Zircon crystals in the AD1 diorite ($\delta^{18}\text{O}(\text{WR}) = 7.0 \pm 0.4 \text{‰}$ (n=2); $\text{SiO}_2(\text{WR}) = 53.0 \text{ wt}\%$;
329 $\delta^{18}\text{O}(\text{Zrc}) = 7.1 \pm 0.4 \text{‰}$) contain two apparent populations of oxygen isotope values that
330 cannot both be in isotopic equilibrium with the host rock, and in themselves indicate isotopic
331 disequilibrium.

332 A change in $\delta^{18}\text{O}$ (zircon) can only be achieved by adding material of a different oxygen
333 isotope composition to a magma (Valley, 2003), which implies that the two apparent $\delta^{18}\text{O}$
334 populations in the AD1 zircons must represent mixing of at least two components. In most
335 cases where zircon grains show resolvable variation in $\delta^{18}\text{O}$ between different parts of the
336 crystal, this is manifested as an increase in $\delta^{18}\text{O}$ from core to rim reflecting mixing of a
337 higher- $\delta^{18}\text{O}$ melt with the magma. However, the reverse trend has also been observed (grain
338 10), which suggests components less enriched in ^{18}O were also mixed into the magma at some
339 stage. We conclude that the two apparent populations do not represent simple mixing of only
340 two components. Instead, a more complicated scenario is envisaged in which there were at
341 least two melt batches (a high- $\delta^{18}\text{O}$ melt with $\geq 8.1 \text{‰}$ and a lower- $\delta^{18}\text{O}$ melt with $\leq 6.6 \text{‰}$
342 representing the highest and lowest measured zircon values (rim in grain 11 and c2 domain in
343 grain 10, respectively)). Plausibly, multiple batches mixed with the magma *during* zircon
344 growth. Imperfect mixing may also have led to some of the variation observed between zircon
345 crystals. Due to this complicated mixing history we conclude that neither major zircon
346 population in AD1 can have been in equilibrium with the present host rock. Independent
347 textural or geochemical evidence for magma mixing has not been recognised in AD1.

348 The outer rims of zircon crystals are most likely to be in equilibrium with the current host
349 rock. Comparing zircon rim and whole-rock $\delta^{18}\text{O}$ data is complicated as zircon rims fall into
350 low- $\delta^{18}\text{O}$ ($6.1\text{-}6.5 \text{‰}$) (1 grain) and high- $\delta^{18}\text{O}$ ($7.5\text{-}7.6 \text{‰}$) (5 grains) groups. Considering a
351 calculated $\Delta(\text{Zrc-WR})$ value of -0.7‰ ($53.0 \text{ wt}\% \text{SiO}_2$) and the AD1 whole-rock composition
352 of $7.0 \pm 0.4 \text{‰}$, only the low- $\delta^{18}\text{O}$ rims can be in isotopic equilibrium (Fig. 6). To be in
353 equilibrium with the high- $\delta^{18}\text{O}$ rims, the whole-rock oxygen isotope composition would have
354 to lie between 7.8‰ and 8.7‰ , and as high- $\delta^{18}\text{O}$ rims appear to be more common they may

355 be more representative of the bulk magma from which the zircons crystallised. This would
356 suggest that the current host rock underwent later depletion in ^{18}O , possibly by further mixing
357 with low- $\delta^{18}\text{O}$ components, or by hydrothermal alteration, for example by interaction with
358 heated meteoric water (Farver and Giletti, 1989; Smith, 1981) after zircon had crystallised.
359 Since plagioclase and biotite show only minor signs of alteration, any hydrothermal alteration
360 would have occurred at or close to magmatic temperatures. The fact that zircons and whole-
361 rock are in isotopic equilibrium in the CnG diorite suggests that it was unaffected by
362 alteration even though the CnG and AD1 intrusions are located only approximately 1.5 km
363 apart from each other. Hydrothermal fluids typically have heterogeneous flow paths, differing
364 flow durations and fluid/rock ratios, and the intensity of alteration can vary at μm to km
365 scales (Valley and Graham, 1996). Alternatively, isotopic equilibrium between zircon and
366 whole-rock in the CnG diorite is fortuitous.

367

368 5.2. Quartz – zircon equilibrium fractionation

369

370 Quartz in granite is less susceptible to hydrothermal alteration than its whole-rock host,
371 reflecting the susceptibility of feldspar to rapid isotopic exchange with hydrothermal fluid
372 down to temperatures of 300-400°C. Quartz exchanges oxygen isotopes mainly by
373 solution/re-precipitation and by slow temperature-dependent volume diffusion, exploiting
374 fractures and crystal boundaries (Valley and Graham, 1996). Hence, if annealed cracks and
375 obviously altered areas are avoided during analysis, the $\delta^{18}\text{O}$ of zircon and quartz may
376 provide a reliable indication of the state of isotopic equilibrium and of magmatic evolution.

377 In contrast to the zircon oxygen isotope data, $\delta^{18}\text{O}$ (Qtz) analyses from both the CnG and
378 AD1 diorites yield unimodal oxygen isotope populations (Fig. 6). Hence, $\delta^{18}\text{O}$ (Qtz) in AD1
379 and CnG provide no evidence of magma mixing. Examining the equilibrium fractionation
380 between zircon and quartz may potentially explain this phenomenon.

381 Equilibrium oxygen isotope fractionation factors between quartz and zircon ($\Delta(\text{Qtz-Zrc})$)
382 as a function of temperature are given by the empirical equation (Valley et al., 2003):

383

$$384 \quad \delta^{18}\text{O}_{\text{Qtz}} - \delta^{18}\text{O}_{\text{Zrc}} = \Delta_{\text{Qtz-Zrc}} \approx 1000 \ln (\alpha_{\text{Qtz-Zrc}}) = A_{\text{Qtz-Zrc}} 10^6/T^2 \quad (2)$$

385

386 where $A_{\text{Qtz-Zrc}} = 2.64$ (‰K^2); T = temperature in degrees Kelvin.

387

388 At 800°C the equilibrium value of $\Delta(\text{Qtz-Zrc})$ is 2.3 ‰. However, for diorite CnG (mean
389 $\delta^{18}\text{O}(\text{Zrc}) = 6.0 \pm 0.6$, mean $\delta^{18}\text{O}(\text{Qtz}) = 10.9 \pm 0.5$ ‰) the calculated $\Delta(\text{Qtz-Zrc})$ is 4.9 ± 1.1
390 ‰. Due to the complex $\delta^{18}\text{O}(\text{Zrc})$ distribution in AD1, the mean oxygen isotope value of
391 zircon cannot be used for this calculation. Instead we use the lowest and highest measured
392 zircon values ($\delta^{18}\text{O}(\text{Zrc}) = 6.1\text{-}8.1 \pm 0.4$ ‰, mean $\delta^{18}\text{O}(\text{Qtz}) = 11.7 \pm 0.6$ ‰), yielding
393 $\Delta(\text{Qtz-Zrc})$ of $5.6\text{-}3.6 \pm 1.0$ ‰. Taking the error into account, the $\Delta(\text{Qtz-Zrc})$ value is at least
394 1.2 ‰ higher in CnG and 0.3 ‰ higher in AD1 than the calculated value of 2.3 ‰ for isotopic
395 equilibrium at 800°C using equation (2). A temperature of 700°C would permit equilibrium
396 between only the highest $\delta^{18}\text{O}$ -zircons observed in the AD1 diorite and quartz (and only if the
397 error is taken into account). We conclude that zircon and quartz are not in isotopic
398 equilibrium.

399 Other authors (e.g. King and Valley, 2001; Monani and Valley, 2001) have found that
400 quartz does not always preserve magmatic $\delta^{18}\text{O}$ values as robustly as zircon, due to post-
401 magmatic hydrothermal diffusive oxygen exchange and alteration. However, the lack of
402 oxygen isotope heterogeneity along cracks and crystal boundaries or between different quartz
403 crystal sizes in AD1 and CnG suggests that in both samples quartz has essentially retained its
404 oxygen isotope composition from the time of crystallisation and therefore high $\delta^{18}\text{O}(\text{Qtz})$ was
405 not caused by hydrothermal alteration or closed-system exchange with feldspar. We conclude
406 that in the CnG diorite quartz crystallised (or completely recrystallised) from late magmatic or
407 high-temperature post-magmatic (subsolidus) fluids with high $\delta^{18}\text{O}$ after zircon had ceased to
408 crystallise. The analysed zircons may contain a very thin outer rim that is in equilibrium with
409 quartz, but due to the spatial resolution of the ion microprobe this is not detectable. Quartz in
410 AD1 also forms a homogeneous oxygen isotope population in contrast to co-existing zircon,
411 and hence disequilibrium between quartz and zircon, and a similar may also be assumed.

412 In summary, both zircon and quartz in the Lochnagar diorites preserve their oxygen
413 isotope compositions from the time of crystallisation. However, textural and isotopic evidence
414 strongly suggests that zircon and quartz crystallised at different times, and hence we conclude
415 that they represent different magma (or fluid) compositions. As oxygen isotope evidence of
416 magma mixing was only found in AD1 zircons and not in quartz, the $^{18}\text{O}/^{16}\text{O}$ of the AD1
417 magma (or late magmatic fluid) must have been completely homogenised and relatively more
418 ^{18}O -enriched at the stage of quartz crystallisation.

419

420 *5.3. Petrogenetic evolution model*

421

422 The granites and diorites of the Lochnagar pluton belong to a suite of late Caledonian I-
423 type intrusions in Scotland whose protoliths are thought to be “igneous” or “infracrustal”
424 insofar as these protoliths have not experienced a weathering cycle (Chappell and Stephens,
425 1988). I-type granitic rocks are widely considered to be the products of either (1) (re)melting
426 of deep-crustal igneous rocks, implying that they are the products of crustal differentiation
427 and recycling rather than crustal growth; or (2) the interaction (by melting or assimilation) of
428 mantle-derived (mafic) magmas with older crustal rocks, implying the generation and growth
429 of new continental crust (e.g. Kemp and Hawkesworth, 2005).

430 Zircons in equilibrium with pristine mantle melts have $\delta^{18}\text{O}$ of $5.3 \pm 0.6 \text{ ‰}$ (2σ , Valley et al., 1998). This value is insensitive to modification by differentiation since whole-rock $\delta^{18}\text{O}$
431 and $\Delta(\text{melt} - \text{Zrc})$ increase in parallel as differentiation and accompanying increase of SiO_2
432 proceed (Valley et al., 1994). The occurrence of zircons with $\delta^{18}\text{O} > 5.6 \text{ ‰}$ in dioritic rocks
433 thus indicates that the protoliths contained an ^{18}O -enriched supracrustal component or an
434 altered igneous source, and/or represent the the interaction of mantle-derived magmas with
435 supracrustal materials.
436

437 Zircon crystals in the Lochnagar diorites are enriched in ^{18}O by an average of 0.7 ‰ to 2.1
438 ‰ relative to pristine mantle values ($\delta^{18}\text{O}(\text{CnG}) = 6.0 \pm 0.6 \text{ ‰}$; $\delta^{18}\text{O}(\text{AD1}) = 7.1 \pm 0.4 \text{ ‰}$),
439 indicating the involvement of ^{18}O -enriched crustal protoliths (supracrustal rocks or altered
440 igneous rocks) in the their generation or evolution, either as remelted protoliths or by
441 assimilation or mixing of such protoliths in mantle-derived mafic magmas. Evidence for the
442 involvement of mantle-derived melts may be preserved in zircon crystals with $\delta^{18}\text{O} < 5.9 \text{ ‰}$
443 in the CnG diorites that overlap into the mantle field (Fig. 3). These may have crystallised
444 early in the crystallisation history of the CnG diorite in order to capture evidence of a mantle
445 component before any magma mixing processes took place similar to those recorded in diorite
446 AD1. On a wider scale, mafic enclaves in granites and the occurrence of appinites,
447 lamprophyres and rare gabbroic intrusions of late Caledonian (430-400 Ma) age indicate an
448 indirect role for mantle-derived melts in the genesis of the late Caledonian granites in
449 Scotland (Strachan et al., 2002). However, the absence of any persuasive evidence of a
450 pristine mantle source in the $\delta^{18}\text{O}(\text{Zrc})$ data for the Lochnagar diorites suggest an origin
451 dominated by remelting of mafic lower crustal sources and crustal differentiation rather than
452 crustal growth. On the other hand, the $\delta^{18}\text{O}(\text{Zrc})$ values are not strongly ^{18}O -enriched, and a
453 large supracrustal contribution by for example Dalradian Supergroup metasedimentary host
454 rocks can therefore be ruled out.

455 Several models have been proposed for the origin of intermediate and silicic calc-alkaline
456 magmas. These include fractional crystallisation of mantle-derived basalt or basaltic andesite
457 in shallow crustal magma chambers (e.g. Grove et al., 1997; Pichavant, 1992; Sisson and
458 Grove, 1993) or at/close to the Moho (e.g. Annen and Sparks, 2002; Mortazavi and Sparks,
459 2003; Müntener et al., 2001; Prouteau and Scaillet, 2003), and dehydration melting in lower
460 or middle crust induced by intrusion of hot, hydrous, mafic, mantle-derived magma (e.g.
461 Jackson et al., 2003; Petford and Atherton, 1996; Smith and Leeman, 1987). Based on
462 numerical modelling and experimental data Annen and Sparks (2002) have proposed the
463 existence of ‘deep crustal hot zones’ and have recently applied this model (Annen et al.,
464 2006) to the generation of intermediate and silicic igneous rocks in subduction zone settings.

465 The development of deep crustal hot zones results from repeated intrusion of mantle-
466 derived hydrous basalt sills into the lower crust, where melts are generated either by (1)
467 differentiation of the basalt sills to produce residual and more siliceous H₂O-rich melts, or by
468 (2) partial melting of pre-existing crustal rocks (including early basalt sills). Mixing of
469 residual melts (or mafic mantle melts) and crustal partial melts creates a large range of
470 intermediate and silicic melts with variably ¹⁸O-enriched compositions. The efficiency of melt
471 production in deep crustal hot zones largely depends on the amount of intruding basalt, the
472 level of emplacement in the crust, the rate of emplacement and the composition of the lower
473 and middle crust. Residual melts are most efficiently produced by differentiation of basalt at
474 deep crustal levels. In contrast, the largest amounts of crustal partial melts are generated either
475 by random basalt sill injection over extended periods of time at different mid- and lower
476 crustal levels, heating the crust from below and above, or by emplacement of sills at the
477 contact with a fertile upper crust. Thus, the basalt sills predominantly act as a heat source
478 required for generation of crustal partial melts, but do not necessarily represent the dominant
479 component in the generated melts. After melt generation, melts segregate and, depending on
480 their H₂O content, density, viscosity and ascent path, ascend more or less rapidly into shallow
481 reservoirs in the upper crust where they undergo crystallisation by degassing and cooling
482 (Annen et al., 2006).

483 The tectonic setting that led to intrusion of the late Caledonian ‘I-type’ magmatism in
484 Scotland is still controversial. The late Caledonian granites have commonly been linked to a
485 subduction zone setting (Brown, 1991; Brown et al., 1985; Soper, 1986; Stephens and
486 Halliday, 1984; Stephenson et al., 1999; Thirlwall, 1981, 1982, 1988), and more recently a
487 slab-breakoff model has been proposed (Atherton and Ghani, 2002). Based on the complexity
488 of the zircon oxygen isotope data observed in the AD1 diorite magma generation in a ‘deep

489 crustal hot zone' may provide a suitable model to explain the generation of the Lochnagar
490 diorites. As neither CnG nor AD1 diorites contain populations of zircons with pristine mantle
491 $\delta^{18}\text{O}$ signatures the diorites do not appear to have formed by simple closed-system fractional
492 crystallisation of contemporaneous mantle-derived melts. Assimilation and fractional
493 crystallisation may explain the zircon oxygen isotope composition of the CnG diorite.
494 However, the observed increase and decrease in $\delta^{18}\text{O}$ (zircon) with zircon growth in the AD1
495 diorite, which indicates mixing or assimilation of lower and higher $\delta^{18}\text{O}$ materials, is
496 inconsistent with this process. We therefore propose that the diorites formed in a deep crustal
497 hot zone either by (1) mixing of residual melts and crustal partial melts, or by (2) partial
498 melting of a mafic lower crust. Model 1 implies that zircons with mantle-like $\delta^{18}\text{O}$ values
499 represent a contemporary ~ 420 Ma mantle-derived component, hence new crust, whereas in
500 model 2 mantle-like zircons reflect melting of old lower crust with a mantle-like composition,
501 hence crustal differentiation. Based on oxygen isotope data alone it is not possible to
502 distinguish between these two models, but due to the overall small number of mantle-like
503 zircons crustal recycling appears to have been the dominant process.

504 Valuable information was also gained about the magmatic evolution of the dioritic
505 magmas, which appear to differ significantly. The homogeneity in $\delta^{18}\text{O}$ of the CnG zircons
506 suggests they precipitated from a single homogeneous magma and did not experience open-
507 system processes during zircon growth. In contrast, the AD1 magma experienced *at least* two
508 mixing events involving a high $\delta^{18}\text{O}$ (≥ 8.1 ‰) and a lower- $\delta^{18}\text{O}$ melt (≤ 6.6 ‰). As these
509 mixing events appear to have occurred during zircon growth, they probably took place at
510 shallow crustal levels after ascent. The juxtaposition of two or more magmas of differing $\delta^{18}\text{O}$
511 is consistent with a model of incremental assembly of melt batches in the AD pluton.
512 Resorption surfaces between cores and rims or between mantles do not appear to represent the
513 timing of mixing as (1) a shift in $\delta^{18}\text{O}$ between cores and rims was not always observed, (2)
514 variations in $\delta^{18}\text{O}$ exist within single zones, and (3) zircons from both the CnG and AD1
515 diorites contain resorption surfaces, but no evidence of mixing was found in CnG. Thus, these
516 surfaces are more likely to represent local differences in the growth environment due to
517 fluctuations in Zr content. In both diorites quartz crystallised late from homogenised, high-
518 $\delta^{18}\text{O}$ melt or fluid, is thus not in equilibrium with zircon and shows no evidence of magma
519 mixing. After zircon and quartz crystallisation, diorite AD1, and perhaps also the CnG diorite,
520 may have been affected by high-temperature hydrothermal alteration by infiltration of hot
521 meteoric fluids, resulting in a decrease in whole-rock oxygen isotope composition.

522

523

524 **6. Conclusions**

525

526 1) High-precision in-situ SIMS oxygen isotope analysis reveals small ($\ll 1$ ‰) variations in
527 oxygen isotope composition in zircon and quartz crystals in Scottish late Caledonian
528 diorites at a spatial resolution of around 20 μm .

529 2) Zircon in the Cul nan Gad diorite intrusion yields a unimodal distribution of oxygen
530 isotope values with a mean of 6.0 ± 0.6 ‰, whereas zircon in the Allt Darrarie diorite
531 intrusion yields two apparent populations with means of 6.6 ± 0.4 ‰, and 7.4 ± 0.4 ‰.
532 The $\delta^{18}\text{O}$ composition of zircon preserved in growing crystals in the latter diorite can only
533 evolve by open-system changes to the magma composition, so the presence of two
534 populations of oxygen isotope values in zircon represents a cryptic record of magma
535 mixing during zircon crystallisation. Detailed examination of the grain-scale variations
536 reveals increases as well as decreases in $\delta^{18}\text{O}$ with zircon growth. This suggests that the
537 two apparent populations do not represent simple mixing between two components, but
538 indicates a more complicated process involving additional magma component(s).

539 3) Quartz oxygen isotope data show no evidence of a mixing event. Evaluation of $\Delta(\text{Qtz-}$
540 $\text{Zrc})$ values shows that quartz and zircon are not in equilibrium in either diorite host. This
541 is interpreted to reflect quartz crystallisation late in the sequence, at lower temperatures
542 and from a higher- $\delta^{18}\text{O}$ magma well after the mixing events in the Allt Darrarie magma.

543 4) Whole-rock and zircon oxygen isotope values appear to be in equilibrium in the Cul nan
544 Gad diorite, although this may be fortuitous. In the Allt Darrarie diorite, the whole-rock
545 $\delta^{18}\text{O}$ value is too low, which indicates that it experienced further mixing or more likely
546 hydrothermal alteration that did not affect either zircon or quartz.

547 5) The Lochnagar diorites are thought to have been generated in a 'deep crustal hot zone' by
548 either (1) mixing of residual melts and crustal partial melts indicating that they
549 incorporate new crust, or (2) melting of mafic lower crustal rocks, indicating crustal
550 recycling. Based on oxygen isotope data alone it is not possible to distinguish between
551 these two models, but the small number of zircons with mantle-like $\delta^{18}\text{O}$ values is
552 consistent with an origin dominated by crustal differentiation rather than crustal growth. A
553 large supracrustal contribution can be ruled out.

554 6) Zircons from the Cul nan Gad diorite crystallised from a homogeneous melt; its magma
555 did not experience open-system changes during zircon growth. Allt Darrarie diorite
556 zircons experienced at least two mixing events during zircon growth.

557 7) A combined zircon, quartz and whole-rock oxygen isotope approach is a powerful way to
558 constrain the petrogenetic evolution of plutons from early crystallisation to late alteration.
559 However, only high-precision in-situ ion microprobe analysis of zircon is capable of
560 revealing the cryptic record of multiple magma mixing events observed in the Allt
561 Darrarie diorite.

562

563

564 **Acknowledgements**

565

566 Funding for this study was provided by a BGS-UCAC grant. S.K.A. acknowledges receipt
567 of doctoral scholarships from Gottlieb Daimler- und Karl Benz-Stiftung, DAAD (German
568 Academic Exchange Service), and the School of GeoSciences, University of Edinburgh. The
569 Edinburgh Ion Microprobe Facility is supported by NERC. We thank John Craven for training
570 and assistance on the Cameca ims-1270 and discussion of the zircon and quartz oxygen
571 isotope data, David Steele for supervision on electron microprobe analysis, Nicola Cayzer and
572 Paula McDade for assistance on the SEM, Nic Odling for major element XRF data, Tony
573 Fallick for whole-rock oxygen isotope data, Mike Hall for helping with zircon mounts and
574 thin sections, and Angus Calder for assisting during grain separation. Helpful and constructive
575 reviews by two anonymous reviewers are gratefully acknowledged. M.R.G. writes with
576 permission of the Director of the British Geological Survey.

577

578

579 **References**

580 Annen, C., Blundy, J.D., Sparks, R.S.J., 2006. The genesis of intermediate and silicic magmas
581 in deep crustal hot zones. *J. Petrol.* 47, 505-539.

582 Annen, C., Sparks, R.S.J., 2002. Effects of repetitive emplacement of basaltic intrusions on
583 thermal evolution and melt generation in the crust. *Earth Planet. Sci. Lett.* 203, 937-955.

584 Atherton, M.P., Ghani, A.A., 2002. Slab breakoff: a model for Caledonian, Late Granite syn-
585 collisional magmatism in the orthotectonic (metamorphic) zone of Scotland and Donegal,
586 Ireland. *Lithos* 62, 65-85.

587 Bindemann, I.N., Valley, J.W., 2001. Low $\delta^{18}\text{O}$ rhyolites from Yellowstone: Magmatic
588 evolution based on analysis of zircons and individual phenocrysts. *J. Petrol.* 42, 1491-
589 1517.

590 Brown, G.C., Francis, E.H., Kennan, P. Stillman, C.J., 1985. Caledonian igneous rocks of
591 Britain and Ireland, in: Harris, A.L. (Ed.), The Nature and Timing of Orogenic Activity in
592 the Caledonian Rocks of the British Isles. Geological Society, London, pp. 1-15.

593 Brown, P.E., 1991. Caledonian and earlier magmatism, in: Craig, G.Y. (Ed.), Geology of
594 Scotland, third ed. Geological Society, London, pp. 229-295.

595 Cavosie, A.J., Valley, J.W., Wilde, S.A., E.I.M.F., 2005. Magmatic $\delta^{18}\text{O}$ in 4400-3900 Ma
596 detrital zircons: A record of the alteration and recycling of the crust in the Early Archean.
597 Earth Planet. Sci. Lett. 235, 663-681.

598 Chappell, B.W., Stephens, W.E., 1988. Origin of infracrustal (I-type) granite magmas. Trans.
599 Roy. Soc. Edinburgh, Earth Sciences. 79, 71-86.

600 Corfu, F., Hanchar, J.M., Hoskin, P.W.O., Kinny, P., 2003. Atlas of zircon textures, in:
601 Hanchar, J.M., Hoskin, P.W.O (Eds.), Zircon, Mineralogical Society of America Reviews
602 in Mineralogy & Geochemistry, Washington, 53, 468-500.

603 Coward, M.P., 1990. The Precambrian, Caledonian and Variscan framework to NW Europe,
604 in: Hardman, R.F.P., Brooks, J. (Eds.), Tectonic Events Responsible for Britain's Oil and
605 Gas Reserves, Geological Society, London, Spec. Publ., pp. 1-34.

606 Criss, R.E., Taylor, H.P. Jr., 1986. Meteoric- hydrothermal systems, in: Valley, J.W., Taylor,
607 H.P. Jr., O'Neil, J.R. (Eds.), Stable isotopes in high temperature geological processes,
608 Mineralogical Society of America Reviews in Mineralogy 16, 373-424

609 Dallmeyer, R.D., Strachan, R.A., Rogers, G., Watt, G.R., Friend, C.R.L., 2001. Dating
610 deformation and cooling in the Caledonian thrust nappes of north Sutherland, Scotland:
611 insights from $^{40}\text{Ar}/^{39}\text{Ar}$ and Rb-Sr chronology. J. Geol. Soc., London 158, 501-512.

612 Dewey, J.F., Mange, M., 1999. Petrography of Ordovician and Silurian sediments in the
613 western Irish Caledonides: tracers of a short-lived Ordovician continent-arc collision
614 orogeny and the evolution of the Laurentian-Appalachian-Caledonian margin, in:
615 MacNiociall, C., Ryan, P.D. (Eds.), Continental Tectonics. Geological Society, London
616 Spec. Publ., pp. 55-107.

617 Dodson, M.H., 1973. Closure temperature in cooling geochronological and petrological
618 systems. Contrib. Mineral. Petrol. 40, 259-274.

619 Dowty, E., 1980. Crystal growth and nucleation theory and the numerical simulation of
620 igneous crystallization, in: Hargraves, R.B. (Ed.), Physics of Magmatic Processes.
621 Princeton University Press, Princeton, New Jersey, pp. 419-485.

622 Farver, J.R., Yund, R.A., 1991. Oxygen diffusion in quartz; dependence on temperature and
623 water fugacity. Chem. Geol. 90, 55-70.

624 Grove, T.L., Donnelly-Nolan, J.M., Housh, T., 1997. Magmatic processes that generated the
625 rhyolite Glass Mountain, Medicine Lake volcano, N California. *Contrib. Mineral. Petrol.*
626 127, 205-223.

627 Halliday, A.N., 1984. Coupled Sm-Nd and U-Pb systematics in late Caledonian granites and
628 the basement under northern Britain. *Nature* 307, 229-233.

629 Halliday, A.N., Aftalion, M., van Breemen, O., Jocelyn, J., 1979. Petrogenetic significance of
630 Rb-Sr and U-Pb isotopic systems in the 400 Ma old British Isles granitoids and their hosts.
631 In: Harris, A.L., Holland, C.H., Leake, B.E. (Eds.), *The Caledonides of the British Isles -*
632 *Reviewed.* Geological Society, London Special Publications, pp. 653-662.

633 Jackson, M.D., Cheadle, M.J., Atherton, M.P., 2003. Quantitative modeling of granitic melt
634 generation and segregation in the continental crust. *J. Geophys. Res.* 108, 2332.

635 Kemp, A.I.S., Hawkesworth, C.J., 2005. Granitic perspectives on the generation and secular
636 evolution of the continental crust, in: Rudnick, R.L. (Ed.), *The Crust, Treatise on*
637 *Geochemistry*, Elsevier, pp. 349-410.

638 Kemp, A.I.S., Hawkesworth, C.J., Foster, G.L., Paterson, B.A., Woodhead, J.D., Hergt, J.M.,
639 Gray, C.M., Whitehouse, M.J., 2007. Magmatic and crustal differentiation history of
640 granitic rocks from Hf-O isotopes in zircon. *Science* 315, 980-983.

641 Kemp, A.I.S., Hawkesworth, C.J., Paterson, B.A., Kinny, P.D., 2006. Episodic growth of the
642 Gondwana supercontinent from hafnium and oxygen isotopes in zircon. *Nature* 439, 580-
643 583.

644 Kemp, A.I.S., Whitehouse, M.J., Hawkesworth, C.J., Alarcon, M.K., 2005a. A zircon U-Pb
645 study of metaluminous (I-type) granites of the Lachlan Fold Belt, southeastern Australia:
646 implications for the high/low temperature classification and magma differentiation
647 processes. *Contrib. Mineral. Petrol.* 150, 230-249.

648 Kemp, A.I.S., Wormald, R.J., Whitehouse, M.J., Price, R.C., 2005b. Hf isotopes in zircon
649 reveal contrasting sources and crystallization histories for alkaline to peralkaline granites
650 of Temora, southeastern Australia. *Geology* 33, 797-800.

651 King, E.M., Barrie, C.T., Valley, J.W., 1997. Hydrothermal alteration of oxygen isotope
652 ratios in quartz phenocrysts, Kidd Creek mine, Ontario: Magmatic values are preserved in
653 zircon. *Geology* 25, 1079-1082.

654 King, E.M., Beard, B.L., Johnson, C.M., Valley, J.W., 2002. Oxygen and strontium isotopic
655 evidence for the abrupt and steeply-dipping suture between lithospheric plates in the Idaho
656 batholith. *GSA, Abstracts with Programs* 34, 180.

657 King, E.M., Valley, J.W., 2001. The source, magmatic contamination, and alteration of the
658 Idaho batholith. *Contrib. Mineral. Petrol.* 142, 72-88.

659 King, E.M., Valley, J.W., Davis, D.W., 2000. Oxygen isotope evolution of volcanic rocks at
660 the Sturgeon Lake volcanic complex, Ontario. *Canadian J. Earth Science* 37, 39-50.

661 King, E.M., Valley, J.W., Davis, D.W., Edwards, G.R., 1998. Oxygen isotope ratios of
662 Archean plutonic zircons from granite-greenstone belts of the Superior Province: indicator
663 of magmatic source. *Precambrian Res.* 92, 365-387.

664 King, E.M., Valley, J.W., Stockli, D.F., Wright, J.E., 2004. Oxygen isotope trends of granitic
665 magmatism in the Great Basin: Location of the Precambrian craton boundary as reflected
666 in zircons. *GSA Bulletin* 116, 451-462.

667 Kinny, P.D., Strachan, R.A., Rogers, G.R., Friend, C.R.L., Knocks, H., 2003. U-Pb
668 geochronology of deformed meta-granites in central Sutherland, Scotland: evidence for
669 widespread Silurian metamorphism and ductile deformation of the Moine Supergroup
670 during the Caledonian orogeny. *J. Geol. Soc., London* 160, 259-269.

671 Lackey, J.S., 2005. The magmatic and alteration history of the Sierra Nevada batholith as
672 recorded by oxygen isotope ratios in zircon, titanite, garnet, and quartz, PhD Thesis,
673 University of Wisconsin, Madison, WI.

674 Lackey, J.S., Valley, J.W., Hinke, H.J., 2006. Deciphering the source and contamination
675 history of peraluminous magmas using $\delta^{18}\text{O}$ of accessory minerals: examples from garnet-
676 bearing plutons of the Sierra Nevada batholith. *Contrib. Mineral. Petrol.* 151, 20-44.

677 Lackey, J.S., Valley, J.W., Salleby, J.B., 2005. Supracrustal input to magmas in the deep crust
678 of Sierra Nevada batholith: Evidence from high- $\delta^{18}\text{O}$ zircon. *Earth Planet. Sci. Lett.* 235,
679 315-330.

680 Ludwig, K.R., 2003. *Isoplot 3.00*. Berkeley Geochronology Center Special Publication No. 4

681 Macaulay, C.I., Fallick, A. E., Haszeldine, R. S., Graham, C. M., 2000. Methods of laser-
682 based stable isotope measurement applied to diagenetic cements and hydrocarbon
683 reservoir quality. *Clay Minerals* 35, 313-322.

684 Monani, S., Valley, J.W., 2001. Oxygen isotope ratios of zircon: magma genesis of low $\delta^{18}\text{O}$
685 granites from the British Tertiary Igneous Province, western Scotland. *Earth Planet. Sci.*
686 *Lett.* 184, 377-392.

687 Mortazavi, M., Sparks, R.S.J., 2004. Origin of rhyolite and rhyodacite lavas and associated
688 mafic inclusions of Cape Akrotiri, Santorini: the role of wet basalt in generating
689 calcalkaline silicic magmas. *Contrib. Mineral. Petrol.* 146, 397-413.

690 Müntener, O., Kelemen, P.B., Grove, T.L., 2001. The role of H₂O during crystallisation of
691 primitive arc magmas under uppermost mantle conditions and genesis of igneous
692 pyroxenites: an experimental study *Contrib. Mineral. Petrol.* 141, 643-658.

693 National Institute of Standards & Technology, 1992. Reference Materials 8543-8546

694 Oldershaw, W., 1974. The Lochnagar granitic ring complex, Aberdeenshire. *Scot. J. Geol.* 10,
695 297-309.

696 Peck, W.H., Valley, J.W., Graham, C.M., 2003. Slow oxygen diffusion rates in igneous
697 zircons from metamorphic rocks. *Am. Mineral.* 88, 1003-1014.

698 Peck, W.H., Valley, J.W., Wilde, S.A., Graham, C.M., 2001. Oxygen isotope ratios and rare
699 earth elements in 3.3 to 4.4 Ga zircons: Ion microprobe evidence for high $\delta^{18}\text{O}$ continental
700 crust and oceans in the Early Archean. *Geochim. Cosmochim. Acta.* 65, 4215-4229.

701 Petford, N., Atherton, M., 1996. Na-rich partial melts from newly underplated basaltic crust:
702 the Cordillera Blanca Batholith, Peru. *J. Petrol.* 37, 1491-1521.

703 Pichavant, M., Martel, C., Bourdier, J.L., Scaillet, B., 2002. Physical conditions, structure,
704 and dynamics of a zoned magma chamber: Mount Pelé (Martinique, Lesser Antilles Arc).
705 *J. Geophys. Res.* 107, 2093.

706 Prouteau, G., Scaillet, B., 2003. Experimental constraints on the origin of the 1991 Pinatubo
707 dacite. *J. Petrol.* 44, 2203-2241.

708 Scherer, E., Münker, C., Mezger, K., 2001. Calibration of the Lutetium-Hafnium Clock.
709 *Science* 293, 683-687.

710 Sharp, Z.D., 1990. A laser-based microanalytical method for the in situ determination of
711 oxygen isotope ratios of silicates and oxides. *Geochim. Cosmochim. Acta.* 54, 1353-1357.

712 Sisson, T.W., Grove, T.L., 1993. Experimental investigations of the role of H₂O in calc-
713 alkaline differentiation and subduction zone magmatism. *Contrib. Mineral. Petrol.* 113,
714 143-166.

715 Smith, B.M., 1981. Oxygen and strontium isotopic studies of the Skye intrusive complex,
716 Northwest Scotland, PhD Thesis, Brown University, Providence, RI.

717 Smith, C.G., Goodman, S., Robertson, S., 2001. Geology of the Ballater district. British
718 Geological Survey - Memoir for 1:50 000 Geological Sheet 65E (Scotland).

719 Smith, D.R., Leeman, W.P., 1987. Petrogenesis of Mount St. Helens dacitic magmas. *J.*
720 *Geophys. Res.* 92, 10313-10334.

721 Soper, N.J., 1986. The Newer Granite problem: a geotectonic view. *Geol. Mag.* 123, 227-236.

722 Stephens, W.E., Halliday, A.N., 1984. Geochemical contrasts between late Caledonian
723 granitoid plutons of northern, central and southern Scotland. *Trans. Roy. Soc. Edinburgh:*
724 *Earth Sciences* 75, 259-273.

725 Stephenson, D.B., R.E., Millward, D., Highton, A.J., Parsons, I., Stone, P., Wadsworth, W.J.,
726 2000. Caledonian igneous rocks of Great Britain. *Geological Conservation Review Series*,
727 17. Joint Nature Conservation Committee, pp. 1-648.

728 Strachan, R.A., Smith, M., Harris, A.L., Fettes, D.J., 2002. The Northern Highland and
729 Grampian terranes, in: Trewin, N.H. (Ed.), *The Geology of Scotland*. The Geological
730 Society, London, pp. 81-148.

731 Thirlwall, M.F., 1981. Implications for Caledonian plate tectonic models of chemical data
732 from volcanic rocks of the British Old Red Sandstone. *J. Geol. Soc., London*. 138, 123-
733 138.

734 Thirlwall, M.F., 1982. Systematic variation in chemistry and Nd-Sr isotopes across a
735 Caledonian calc alkaline volcanic arc: implications for source materials. *Earth Planet. Sci.*
736 *Lett.* 58, 27-50.

737 Thirlwall, M.F., 1988. Geochronology of Late Caledonian Magmatism in northern Britain. *J.*
738 *Geol. Soc., London*. 145, 951-967.

739 Valley, J.W., Chiarenzelli, J.R., McLelland, J.M., 1994. Oxygen isotope geochemistry of
740 zircon. *Earth Planet. Sci. Lett.* 126, 187-206.

741 Valley, J.W., Graham, C., 1996. Ion microprobe analysis of oxygen isotope ratios in quartz
742 from Skye granite: healed micro-cracks, fluid flow, and hydrothermal exchange. *Contrib.*
743 *Miner. Petrol.* 124, 225-234.

744 Valley, J.W., Graham, C.M., Harte, B., Eiler, J.M., Kinny, P.D., 1998. Ion microprobe
745 analysis of oxygen, carbon and hydrogen isotope ratios, in: McKibben, M., Shanks, W.,
746 Ridley, I. (Eds.), *Applications of Microanalytical Techniques to Understanding*
747 *Mineralizing Processes*, *Soc. Econ. Geol. Rev. Econ. Geol.* 7, 73-97.

748 Valley, J.W., 2003. Oxygen isotopes in zircon, in: Hanchar, J.M., Hoskin, P.W.O (Eds.),
749 *Zircon, Mineralogical Society of America Reviews in Mineralogy & Geochemistry*,
750 Washington, 53, 343-385.

751 Valley, J.W., Bindemann, I.N., Peck, W.H., 2003. Empirical calibration of oxygen isotope
752 fractionation in zircon. *Geochim. Cosmochim. Acta* 67, 3257-3266.

753 Vavra, G., 1990. On the kinematics of zircon growth and its petrogenetic significance: a
754 cathodoluminescence study. *Contrib. Mineral. Petrol.* 106, 90-99.

755 Vavra, G., 1993. A guide to quantitative morphology of accessory zircon. *Chem. Geol.* 110:
756 15-28.

757 Watson, E.B., Cherniak, D.J., 1997. Oxygen diffusion in zircon. *Earth Planet. Sci. Lett.* 148,
758 527-544.

759 Wiedenbeck, M., Hanchar, J.M., Peck, W.H., Sylvester, P., Valley, J., Whitehouse, M.,
760 Kronz, A., Morishita, Y., Nasdala, L., Fiebig, J., Franchi, I., Girard, J.-P., Greenwood,
761 R.C., Hinton, R., Kita, N., Mason, P.R.D., Norman, M., Ogasawara, M., Piccoli, P.M.,
762 Rhede, D., Satoh, H., Schulz-Dobrick, B., Skår, Ø., Spicuzza, M.J., Terada, K., Tindle,
763 A., Togashi, S., Vennemann, T., Xie, Q., Zheng, Y.-F., 2004. Further Characterization of
764 the 91500 Zircon Crystal. *Geostandards and Geoanalytical Research.* 28, 9-39.

765

766

767

768

769

770

771

772

773 **Figure Captions**

774

775 Fig. 1: Geological sketch map of the Lochnagar pluton (after Smith et al., 2001). Lochnagar
776 comprises three main granite (L1, L2, L3) intrusions, several marginal diorite intrusions and
777 late intrusions of microgranite. This paper focuses on the Cul nan Gad (CnG) and Allt
778 Darrarie (AD1) diorites (stars indicate sample locations).

779

780 Fig. 2: CL images of zircon crystals representative of zircons from the CnG and AD1 diorites
781 with oxygen isotope and U-Pb data (circles indicate position of oxygen isotope analyses,
782 ovals of U-Pb analyses; error on $\delta^{18}\text{O}$ is $\pm 0.4\%$ (2σ); scale bar = 50 μm).

783 a) Zircon grain (AD1 grain 11) consisting of large resorbed, weakly luminescent core (c1) and
784 moderately luminescent rim. Note the large increase in $\delta^{18}\text{O}$ between core and rim.

785 b) Crystal (AD1 grain 9) comprises weakly luminescent unzoned inner core (c1), oscillatory
786 zoned outer core (c2) and a rim. Both $\delta^{18}\text{O}$ values are from within c2, but vary by 0.8‰.

787 c) Zircon (AD1 grain 5) shows similar zoning pattern as b), but has two resorption surfaces.

788 Core and rim analyses are identical within error.

789 d) Zoning is similar to b) and c) with c1, c2, mantles and a rim (AD1 grain 10). Here the c1 is
790 1.2‰ higher than c2, thus zoning is opposite to a).

791 e) Zircon grain lacks obvious c1 core domain (AD1 grain 17).

792

793 Fig. 3: Cumulative probability-histograms and grain-scale variation plot of zircon crystals
794 from the CnG diorite.

795 a) CnG zircons show a narrow range in $\delta^{18}\text{O}$ values and a single mode.

796 b) Unimodal distribution can be observed in all crystal parts.

797 c) All data points lie within error of the mean (light-grey area).

798

799 Fig. 4: Cumulative probability-histograms and grain-scale variation plot of zircon crystals
800 from the AD1 diorite.

801 a) AD1 zircons display a much larger range than CnG zircons and an apparent bimodal
802 distribution.

803 b) Data are separated into the different crystal parts; bimodality can be observed in all parts.

804 c) Data are more scattered and not all lie within error of the mean. Prominent inter-grain

805 variation in $\delta^{18}\text{O}$ occurs between e.g. grains 7 and 16, intra-grain variation between inner and

806 outer core (grain 9), core and rim (grain 11). $\delta^{18}\text{O}$ commonly increases with zircon growth
807 except in grain 10. Bin widths of histograms equal 1SD, error bars are 2σ .

808

809 Fig. 5: CL image of representative quartz crystal (CnG, grain 9) with oxygen isotope data.
810 Quartz contains open and re-crystallised cracks as well as lower-CL areas along its grain
811 margins. Error: $\pm 0.5\text{‰}$ (2σ), scale bar = 200 μm .

812

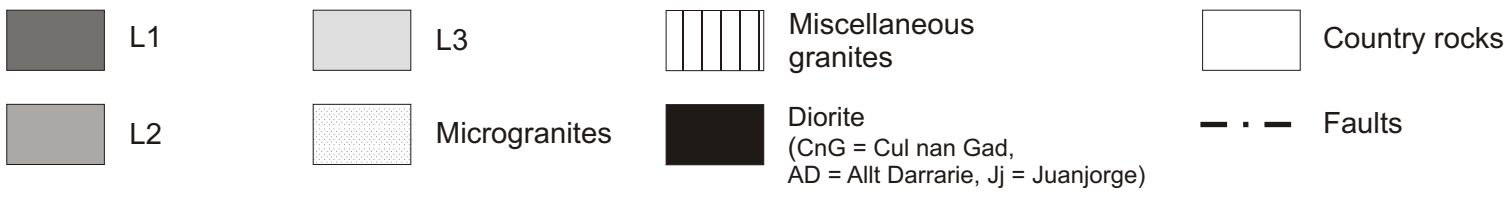
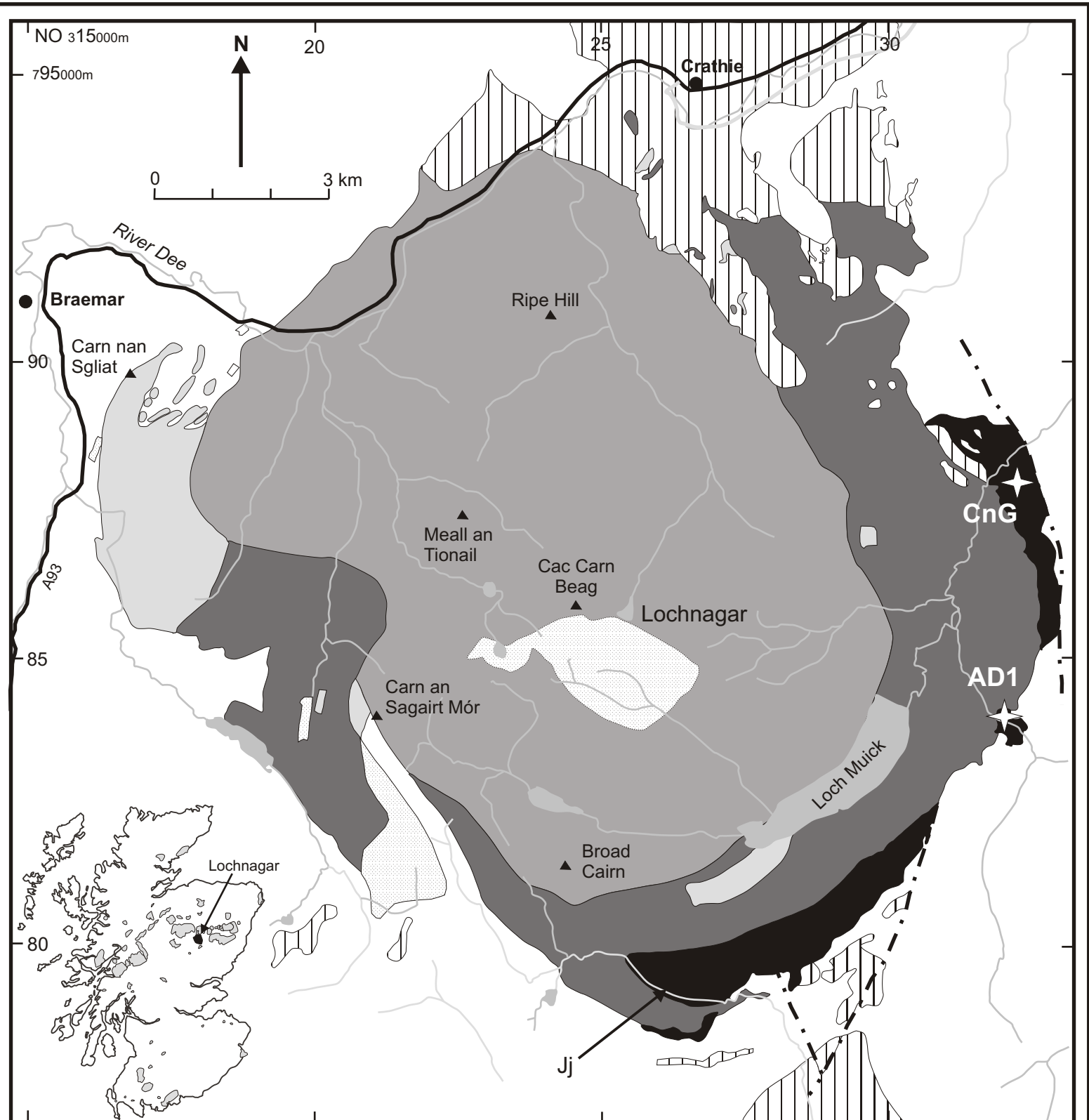
813 Fig. 6: Cumulative probability-histograms of quartz $\delta^{18}\text{O}$ data. Both diorites comprise single
814 quartz populations. Outlier in CnG represents analysis on altered area along a microcrack.

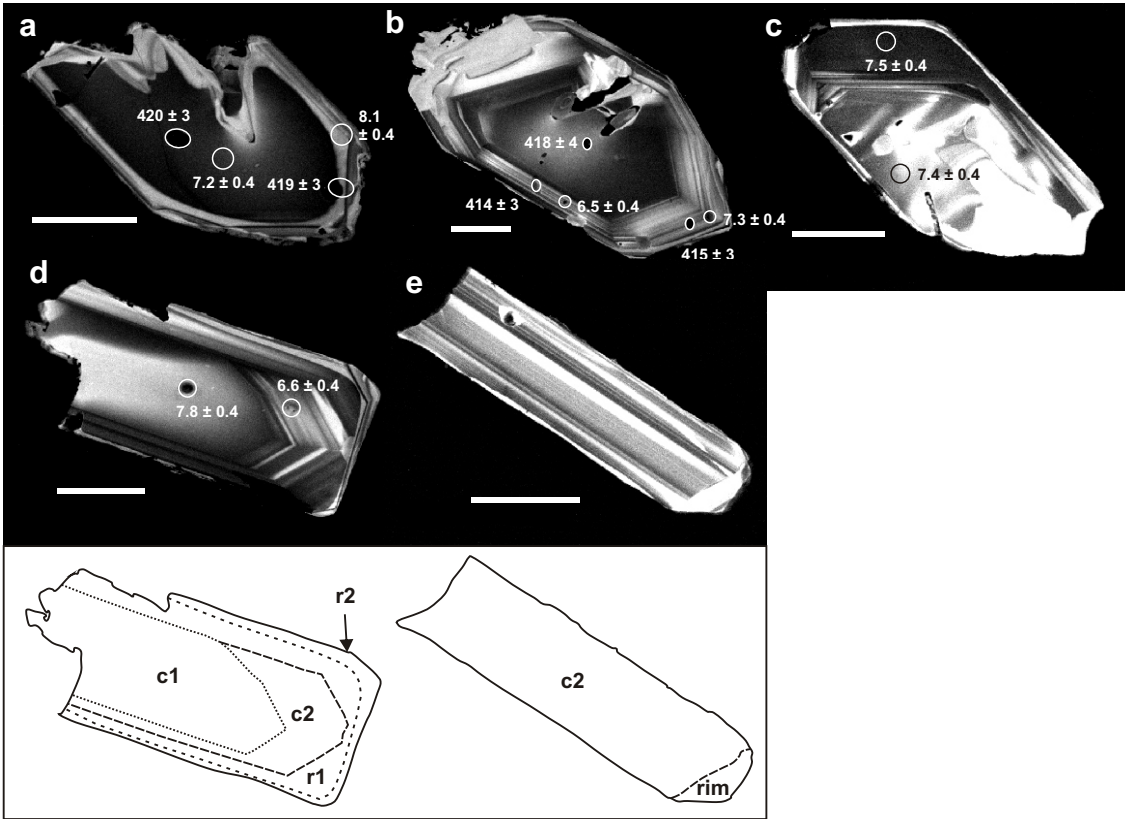
815

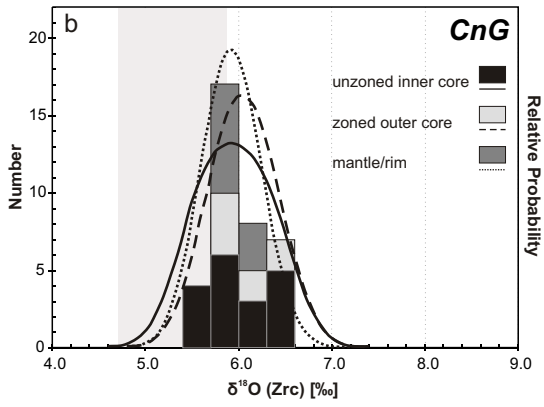
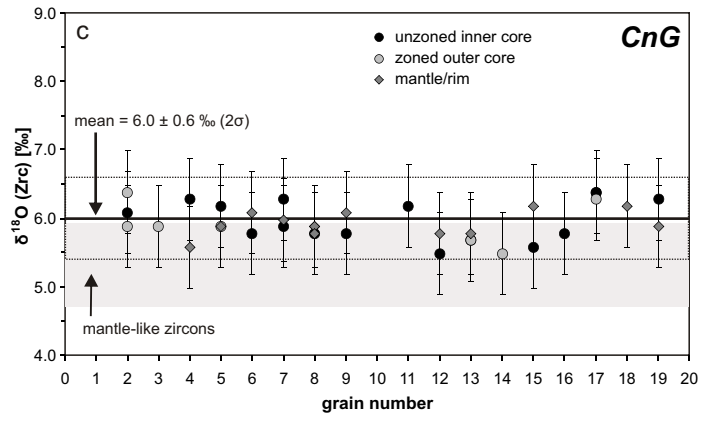
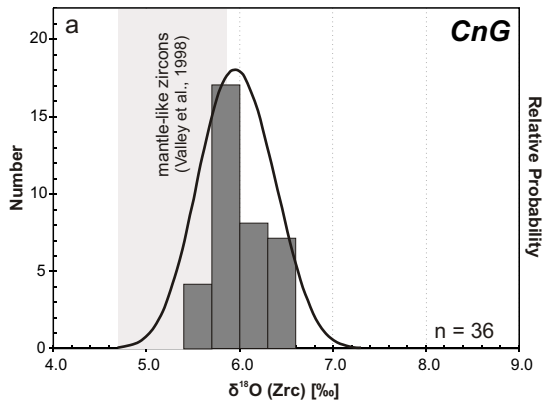
816 Fig. 7: Evaluation of equilibrium between zircon (Zrc), quartz (Qtz) and whole-rock (WR).
817 'Calculated WR' and 'calculated quartz' are calculated using equations (1) and (2) (see text);
818 calculations include the error on the zircon analysis.

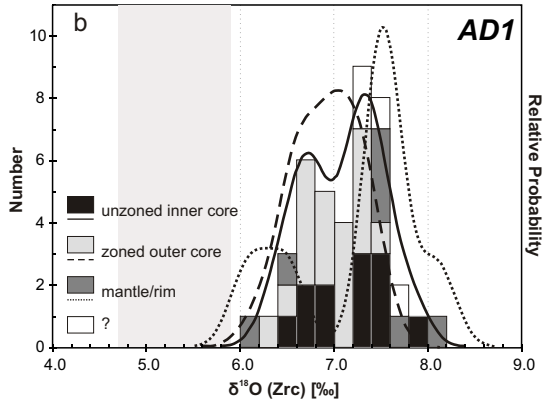
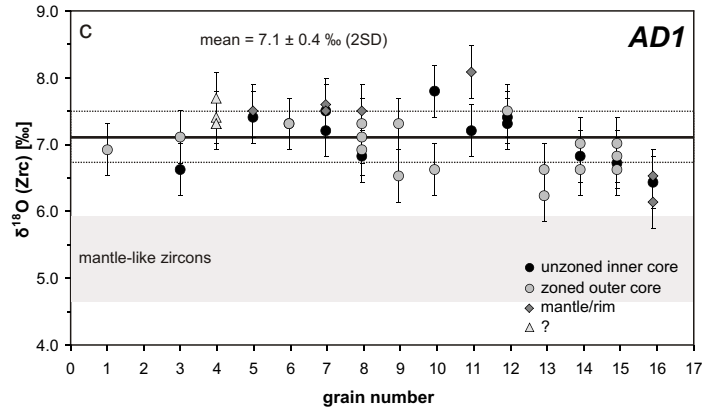
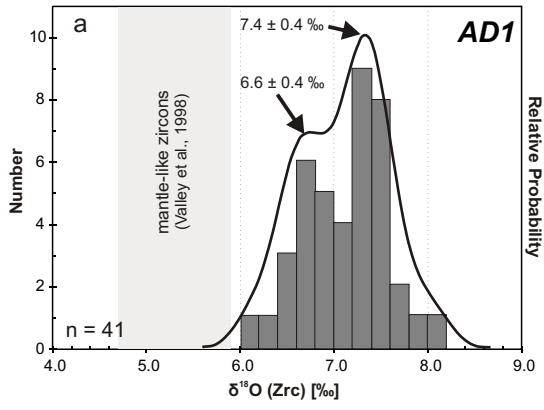
819 AD1: Zircon is not in equilibrium with quartz or whole-rock. Measured whole-rock is too low
820 to be in equilibrium with zircon, which suggests it was affected by hydrothermal alteration
821 after zircon crystallisation.

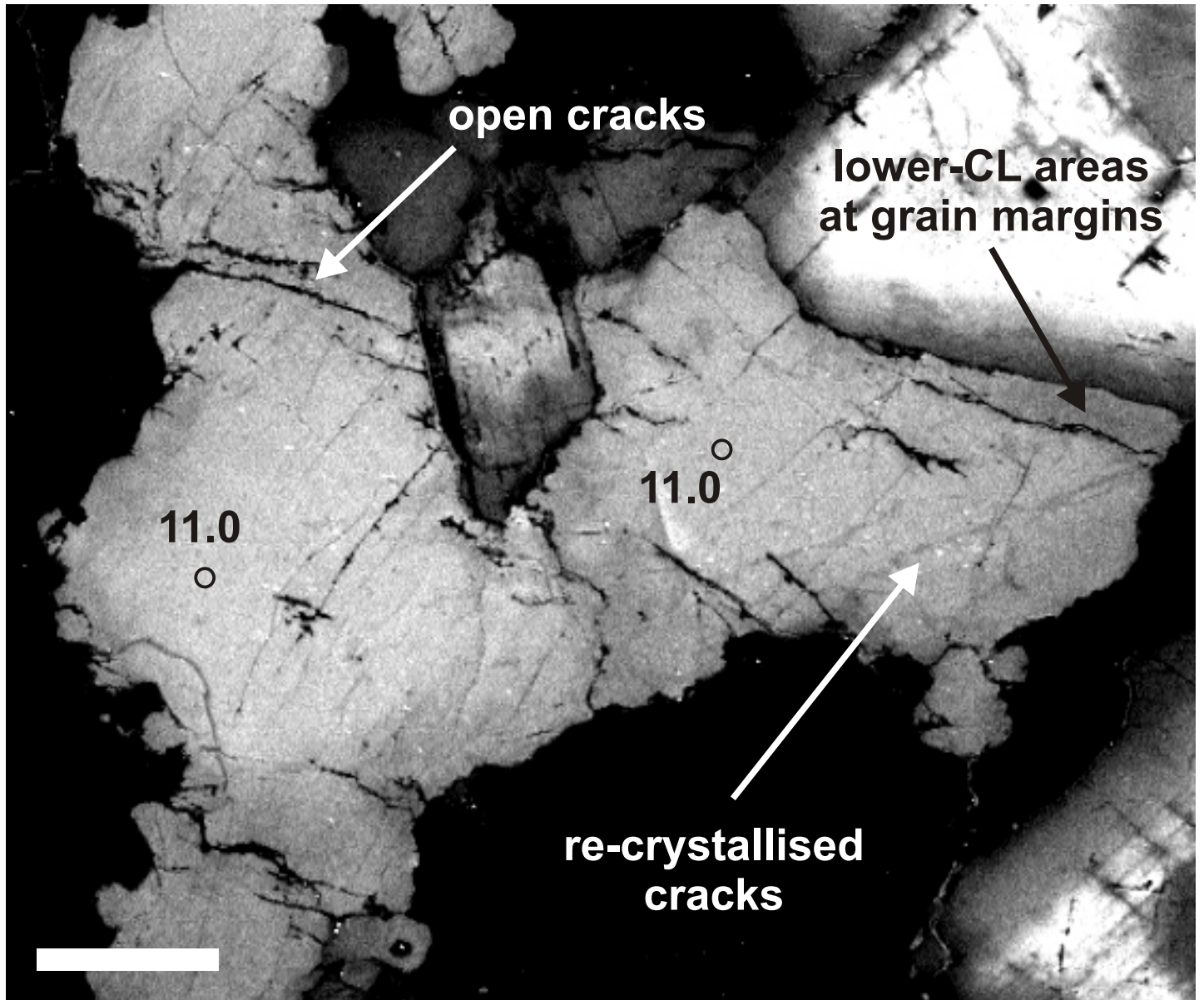
822 CnG: Zircon and quartz are not in equilibrium as measured quartz $\delta^{18}\text{O}$ is considerably higher
823 than the calculated quartz value, which suggests quartz crystallised late in sequence. Zircon
824 and whole-rock are in equilibrium. Low modal percentage of elevated quartz in whole-rock (<
825 5 %) did not shift whole-rock out of equilibrium.











open cracks

lower-CL areas at grain margins

11.0

11.0

re-crystallised cracks

